Methods/Models for estimating Total Particulate Organic Carbon Export

John Dunne NOAA/GFDL

Eppley and Peterson, 1979: Particulate organic matter flux and planktonic new production in the deep ocean. Nature

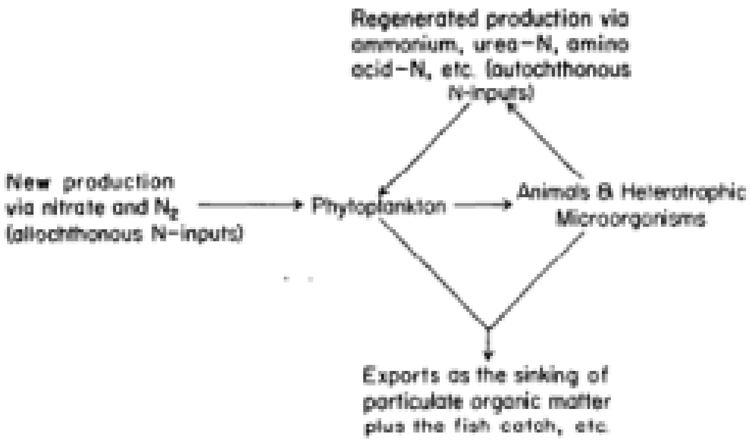

Fig. 1 The production system of the surface ocean, illustrating the concepts of new and regenerated production. Phytoplankton growth is driven by nitrogen inputs of two qualitatively distinct sorts: regenerated and 'new' production. These two pathways leading to phytoplankton production are measured as the phytoplankton assimilation of the various forms of nitrogen using ^{15}N-labelled substrates. This is not possible with other nutrient elements because with carbon or phosphorus, for example, it is not easy to distinguish between autochthonous and allochthonous inputs. To relate new production to export requires that nitrification in the euphotic zone be negligible.

for total production <200 g C m^{-2} yr^{-1}, is described by

$$\text{New/Total} = 0.0025\ (\text{Total}) \qquad (1)$$

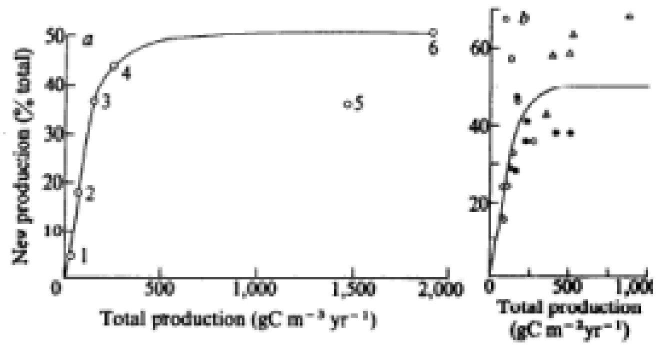

Fig. 2 *a*, New production as % of the total primary production versus total production for various ocean areas: (1) Central North pacific, (2) eastern Mediterranean Sea, (3) Southern California Bight, (4) eastern Tropical Pacific, (5) Costa Rica Dome, and (6) Peru upwelling. Total production was measured by the ^{14}C method. New : total production ratio measurements are based on the assimilation of ^{15}N-labelled nitrate and ammonium. Assimilation of urea and other organic-N was assumed to be either 30% of the total N assimilation[22] or one-half of the ammonium assimilation rate[23]. Results were similar with either correction. No correction was applied for new production as molecular nitrogen fixation as this is assumed to be small[33,34]. Values are regional averages from Dugdale[35] (points 2, 4, 5, 6) and from this laboratory[26] (points 1, 3). The total production rates, from ^{14}C measurements of photosynthesis, are not annual averages but are daily rates × 365 for particular sets of measurements. For example, the annual production of the Peru upwelling area is probably less than the 1,900 C m^{-2} yr^{-1} shown here. *b*, New : total production ratio versus total primary production at individual stations in the Southern California Bight. Nearshore stations in water depth <300 m are omitted. New : total production ratio was calculated as nitrate incorporation rate: (nitrate + 1.5 ammonium incorporation rates). For details see ref. 26. Symbols represent different cruises.

Laws et al., 2000: Temperature effects on export production in the open ocean. GBC

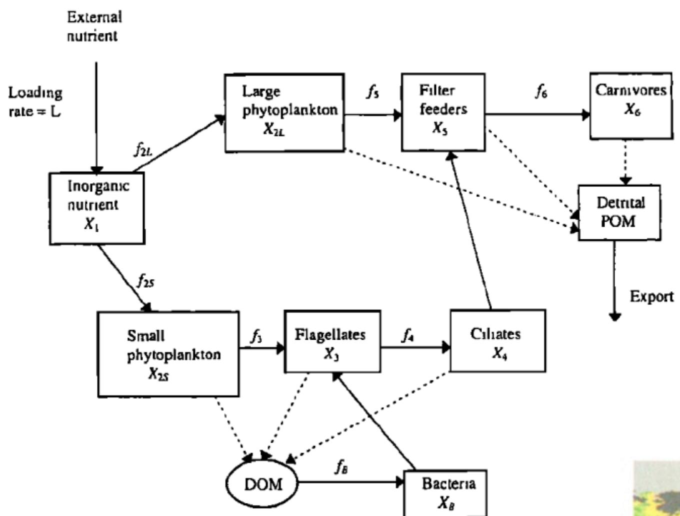

Figure 1. Feeding and excretion relationships in a m food web in which photosynthetic production is between small and large phytoplankton cells.

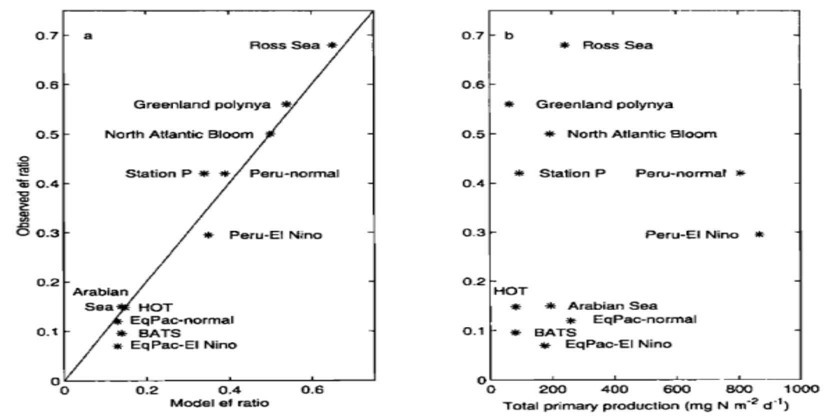

Figure 3. (a) Model ef ratio versus observed ef ratios at locations in Table 3. The straight line is the 1:1 line. (b) Total primary production versus observed ef ratios at the locations in Table 3.

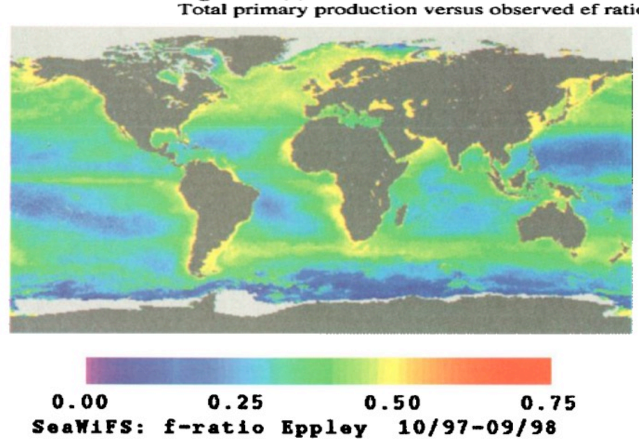

Plate 1. Annual average ef ratios calculated from the EP model. Net photosynthesis was estimated on a monthly basis as described in the text using data collected by the SeaWiFS satellite from October 1997 to September 1998.

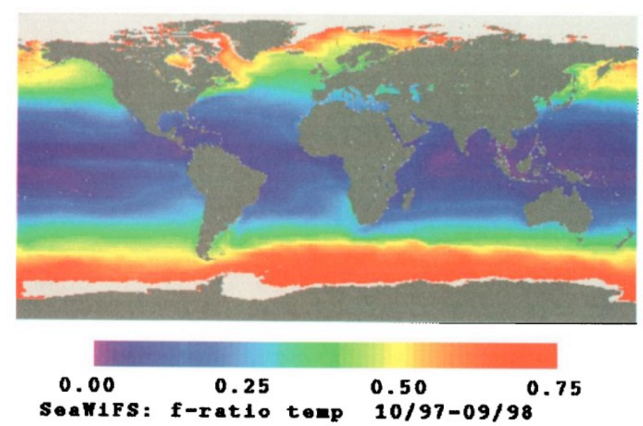

Plate 2. Annual average ef ratios calculated using the TE model Sea surface temperature (SST) fields were derived from monthly AVHRR global data as described in the text

Dunne et al., 2005: Empirical and mechanistic models for the particle export ratio. GBC

Methods include: ^{15}N-new production, Sediment Traps, ^{18}O, O2 change, ^{234}Th, DIC change, biomass change, etc.

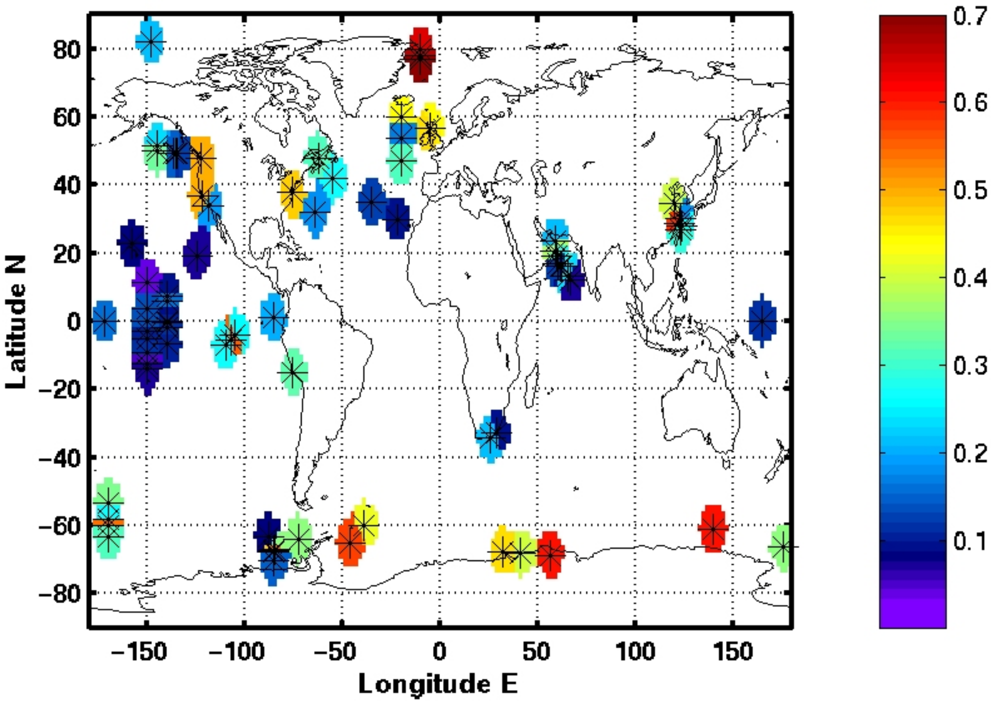

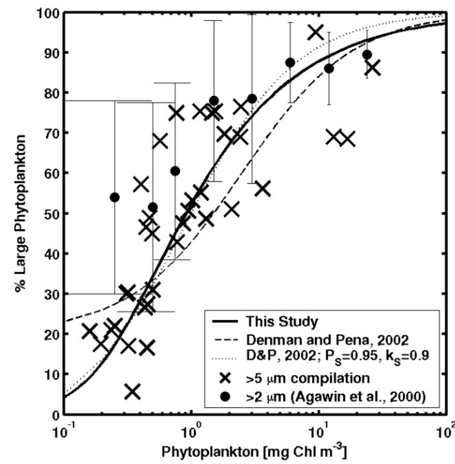

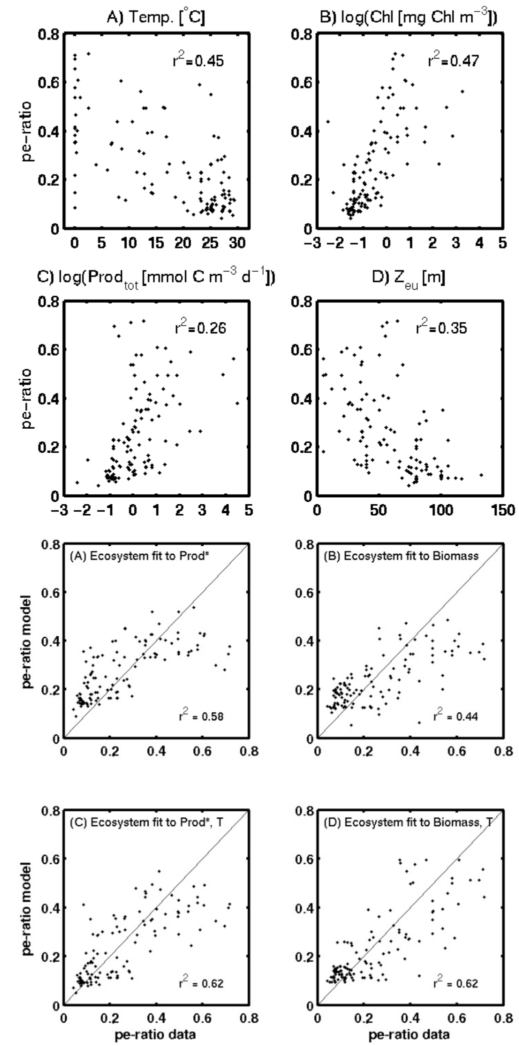

Dunne et al., 2007: A synthesis of global particle export from the surface ocean and cycling through the ocean interior and on the seafloor. GBC

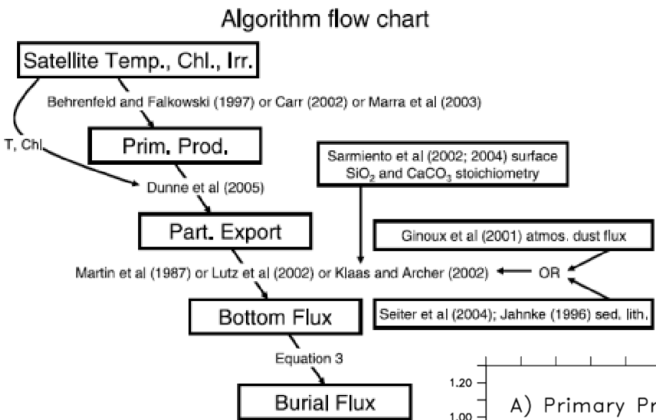

Figure 1. Flow diagram of analysis satellite estimates.

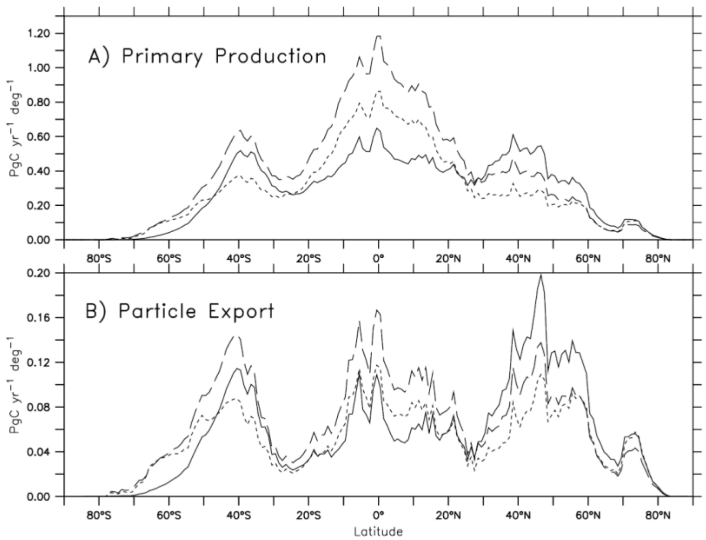

Figure 3. Zonal integrals of primary production (a) and particle export (b) in units of Pg C a^{-1} deg^{-1}. Lines represent the three primary productivity algorithms of *Behrenfeld and Falkowski* [1997] (solid line), *Carr* [2002] (dashed line), and *Marra et al.* [2003] (dotted line).

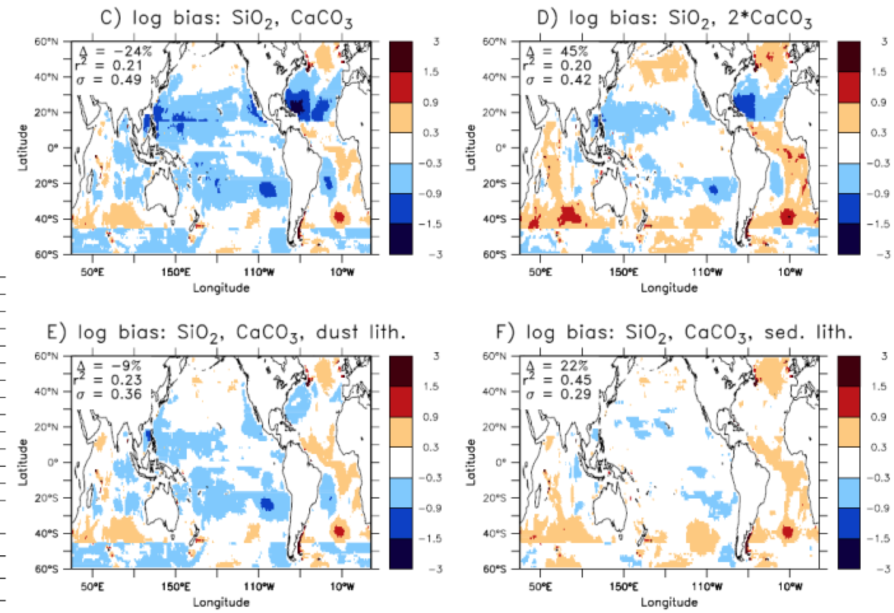

Figure 5. The log10 of the particulate organic carbon flux (mmol m^{-2} d^{-1}) to the seafloor based on sediment derived estimates of benthic oxygen consumption rates from *Jahnke* [1996] converted to organic carbon using a factor of 0.6 plus the sediment POC accumulation rates described in the text (a) used for comparison with satellite-derived estimates in Figures 5b–5f. In each case, the value shown is the log10 ratio of seafloor organic carbon fluxes derived from SeaWiFS satellite over those derived from sediment data syntheses contrasting algorithms for the penetration of POC from the surface to the seafloor (water depths >1000 m; 60°S to 60°N). In all cases, the denominator is the sediment-derived value in Figure 5a. Flux penetration was given by the *Martin et al.* [1987] curve in Figure 5b and variants of the *Klaas and Archer* [2002] parameterization in all the others: (c) Only SiO_2 and $CaCO_3$; (d) as in Figure 5c except with doubling the $CaCO_3$; (e) as in Figure 5c except including lithogenic flux from aeolian dust input of *Ginoux et al.* [2001]; (f) as in Figure 5c except including lithogenic flux derived from the accumulation of lithogenic material in sediments.

Laws et al., 2011: Simple equations to estimate ratios of new or export production to total production from satellite-derived estimates of sea surface temperature and primary production. L&O: Methods

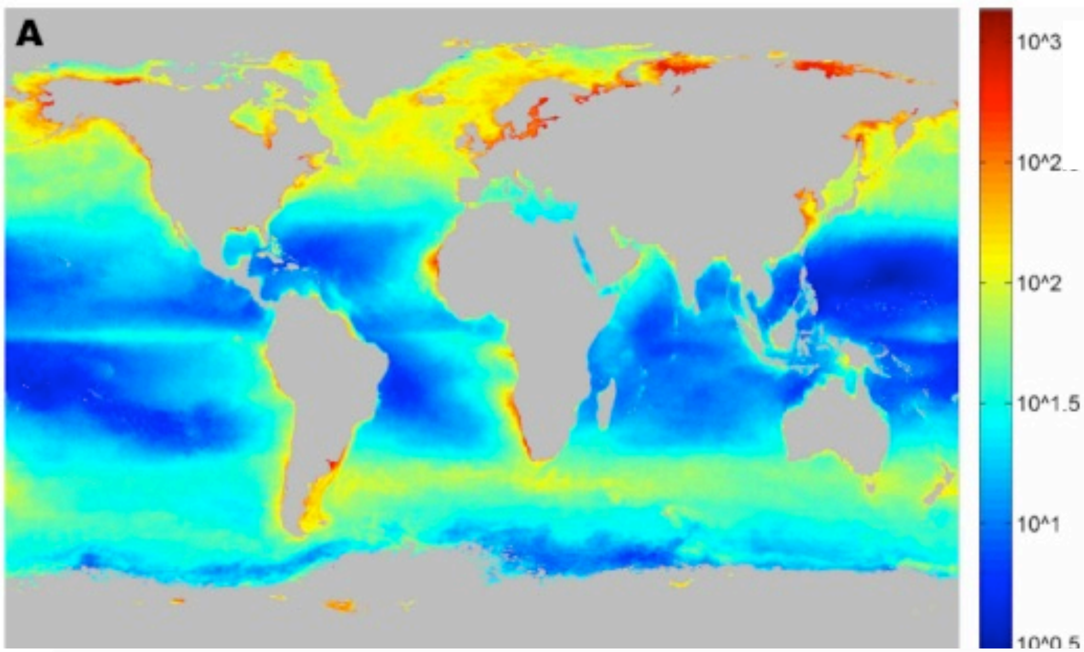

$$ef = 0.04756\left(0.78 - \frac{0.43T}{30}\right)tp^{0.307} \qquad (3)$$

Fig. 5. A: Annual export production (gC/m2) between September 1997 and October 1998 derived from equation. B: Rutgers mask showing different oceanic basins used in deriving the export production.

Henson et al., 2012: Global patterns in efficiency of particulate organic carbon export and transfer to the deep ocean. GBC

Only including 'Particle Export' data, mostly large volume filtration particles

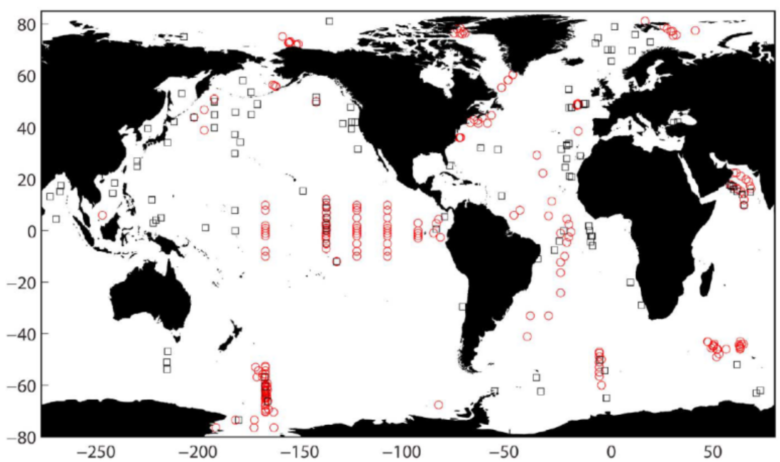

Figure 1. Location of data used in this study. Circles are locations of thorium-based particle export measurements (data in Table S1 in Text S1 in the auxiliary material); squares are locations of POC flux measured using sediment traps [from *Honjo et al.*, 2008].

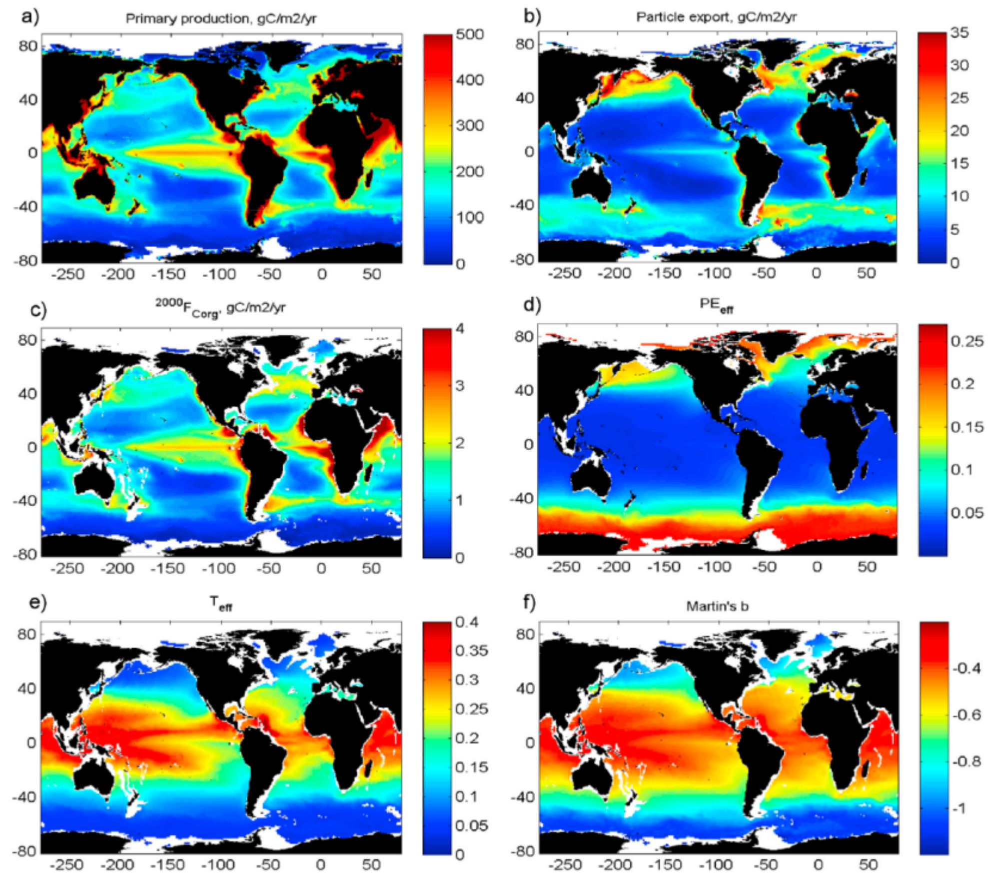

Figure 4. Global maps of satellite-derived (a) primary production estimated from [*Carr*, 2002], (b) POC export at 100 m, (c) POC flux at 2000 m, (d) particle export efficiency (PE_{eff}), (e) transfer efficiency (T_{eff}) and (f) Martin's *b* [*Martin et al.*, 1987].

Siegel et al., 2014: Global assessment of ocean carbon export by combining satellite observations and food-web models. GBC

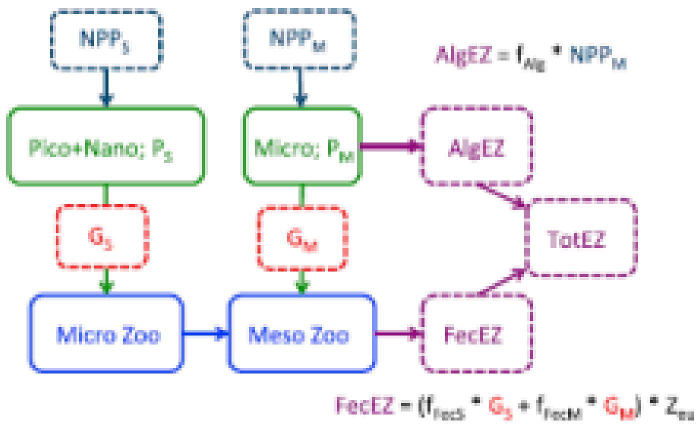

Figure 1. Diagram of the pelagic food web supporting the flux of sinking particles from the euphotic zone (TotEZ). TotEZ is comprised of the flux of sinking intact algal cells (AlgEZ) and the flux of fecal matter from large zooplankton (FecEZ), and they are shown in violet in the diagram. Stocks of phytoplankton are shown in solid green lines and for zooplankton in blue lines. The grazing and NPP fluxes that regulate the stocks are shown in dashed lines and the assumed parameterizations for FecEZ and AlgEZ are given.

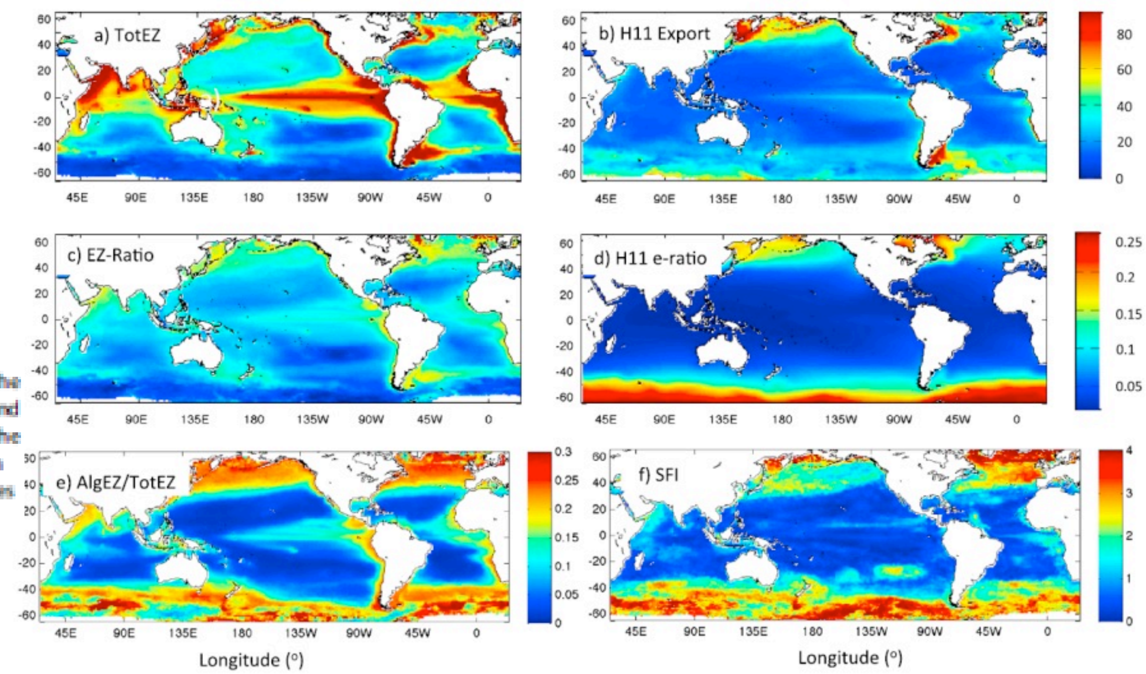

Figure 6. Global distributions of the annual mean (a) $\log_{10}$(TotEZ) (mg C m^{-2} d^{-1}), (b) $\log_{10}$-transormed export flux at 100 m calculated using the H11 e-ratio (mg C m^{-2} d^{-1}), (c) the ratio of TotEZ to NPP, EZ-ratio (unitless), (d) the H11 e-ratio (unitless), (e) ratio of AlgEz to TotEZ (unitless), and (f) seasonal flux index (SFI; unitless).

DeVries and Weber, 2017: The export and fate of organic matter in the ocean: New constraints from combining satellite and oceanographic tracer observations. GBC

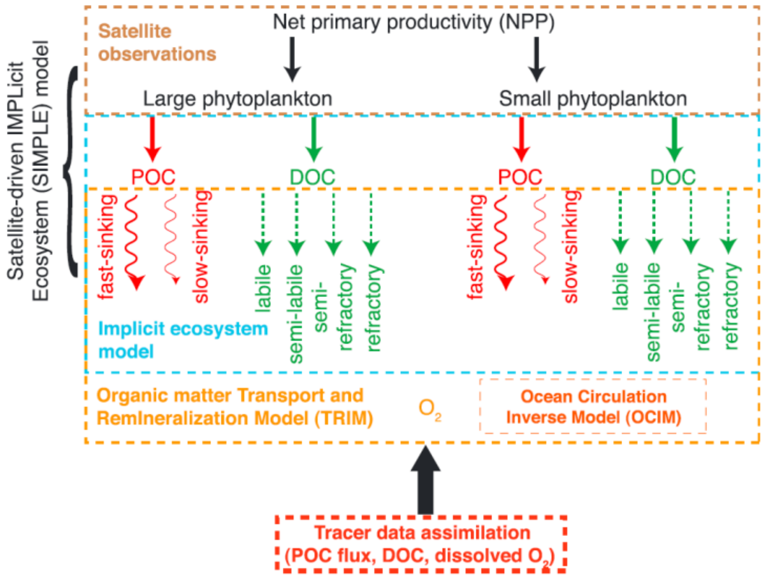

Figure 1. Schematic diagram summarizing the Satellite-driven IMPLicit Ecosystem and organic matter Transport and Remlneralization Model (SIMPLE-TRIM). Satellite observations of NPP and phytoplankton size distribution are used to drive an implicit ocean ecosystem model (SIMPLE) that partitions NPP into particulate (POC) and dissolved (DOC) forms of organic carbon. The ecosystem model is coupled to a model of organic matter transport and remineralization (TRIM), whose ocean circulation component is taken from an offline ocean circulation inverse model (OCIM). Oceanographic tracer observations are assimilated into the model to constrain the SIMPLE-TRIM parameters.

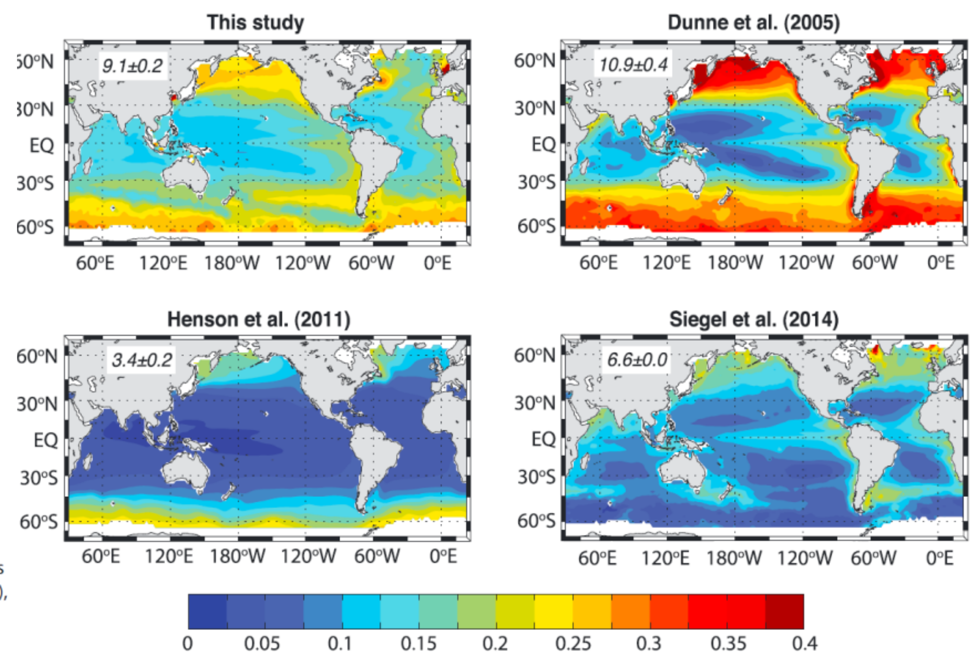

Figure 3. Particle export ratio (ratio of sinking particle flux at the base of the euphotic zone to the NPP at each grid point) for the (top left) SIMPLE-TRIM compared to the empirical models of (top right) *Dunne et al.* [2005] and (bottom left) *Henson et al.* [2011] and the satellite-driven euphotic zone food web model of (bottom right) *Siegel et al.* [2014]. Printed on each map is the globally integrated particle export (Pg C yr^{-1}) for each model. Contour interval is 0.025. For the *Dunne et al.* [2005], *Henson et al.* [2011], and *Siegel et al.* [2014] models, uncertainty in carbon export was estimated by applying the export ratio from each model to the VGPM and CbPM NPP estimates.

DeVries and Weber, 2017: The export and fate of organic matter in the ocean: New constraints from combining satellite and oceanographic tracer observations. GBC

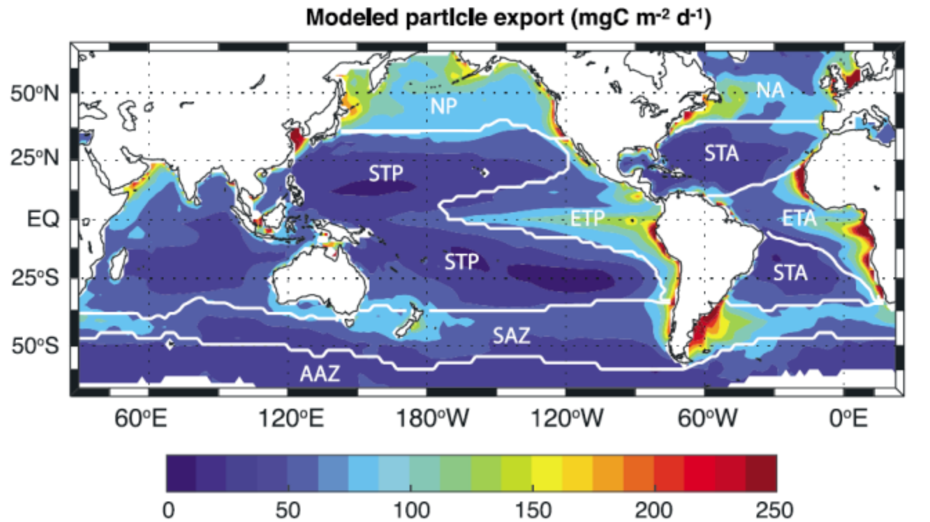

Figure 5. Optimal particle export flux at the base of the euphotic zone from our data-assimilated model. White lines delineate distinct biogeochemical regions defined on the basis of temperature and nutrient concentration [*Weber et al.*, 2016]. AAZ = Antarctic Zone, SAZ = Sub-Antarctic Zone, STA = Subtropical Atlantic, STP = Subtropical Pacific, ETA = Eastern Tropical Atlantic, ETP = Eastern Tropical Pacific, NA = North Atlantic, and NP = North Pacific.

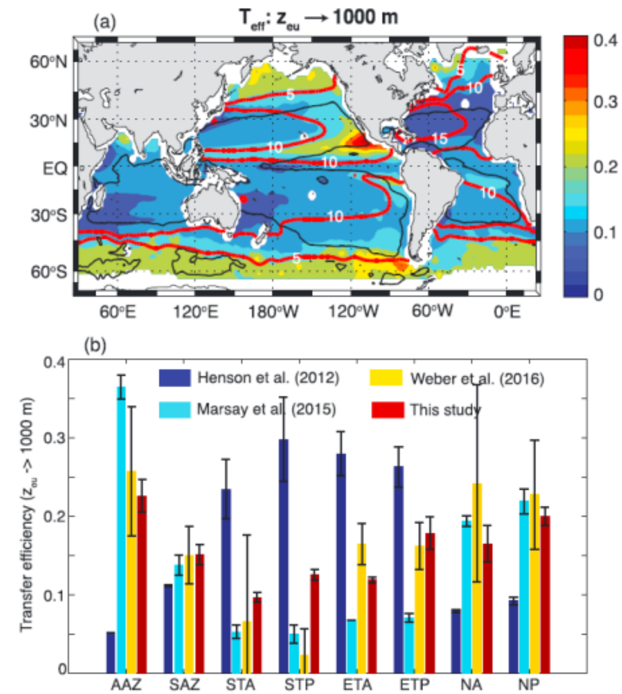

Figure 6. (a) Colors are the transfer efficiency of POC from the base of the euphotic zone to 1000 m from SIMPLE-TRIM. Bold red lines are temperature contours at ~400 m depth (contour interval (CI) 5°C). Thin black lines delineate the surface region containing more than 80% small phytoplankton. (b) Comparison of regionally averaged mesopelagic transfer efficiency from this study and previous studies. Regions as defined in Figure 5. For *Henson et al.* [2012] and *Marsay et al.* [2015], transfer efficiency to 1000 m was mapped using global maps of flux profile exponent (the "Martin parameter") provided by each study. Flux-weighted regional-mean transfer efficiencies were computed, using six different carbon export maps as weighting factors to estimate uncertainty. These combined NPP from VGPM and CbPM with export ratios from *Laws et al.* [2000], *Dunne et al.* [2005], and *Henson et al.* [2011].